The cAMP pathway regulates mRNA decay through phosphorylation of the RNA-binding protein TIS11b/BRF1

Felicitas Rataj†, Séverine Planel†, Agnès Desroches-Castan, Juliette Le Douce, Khadija Lamribet, Josiane Denis, Jean-Jacques Feige, and Nadia Cherradi*

Institut National de la Santé et de la Recherche Médicale, INSERM U1036, Commissariat à l'Energie Atomique et aux Energies Alternatives, Institut de Biosciences et Biotechnologies de Grenoble, Laboratoire Biologie du Cancer et de l'Infection, and Université Grenoble Alpes, Unité Mixte de Recherche-S1036, F-38000 Grenoble, France

ABSTRACT **TPA-inducible sequence 11b/butyrate response factor 1 (TIS11b/BRF1) belongs to the tristetraprolin (TTP) family of zinc-finger proteins, which bind to mRNAs containing AU-rich elements in their 3′-untranslated region and target them for degradation. Regulation of TTP family function through phosphorylation by p38 MAP kinase and Akt/protein kinase B signaling pathways has been extensively studied. In contrast, the role of cAMP-dependent protein kinase (PKA) in the control of TTP family activity in mRNA decay remains largely unknown. Here we show that PKA activation induces TIS11b gene expression and protein phosphorylation. Site-directed mutagenesis combined with kinase assays and specific phosphosite immunodetection identified Ser-54 (S54) and Ser-334 (S334) as PKA target amino acids in vitro and in vivo. Phosphomimetic mutation of the C-terminal S334 markedly increased TIS11b half-life and, unexpectedly, enhanced TIS11b activity on mRNA decay. Examination of protein–protein interactions between TIS11b and components of the mRNA decay machinery revealed that mimicking phosphorylation at S334 enhances TIS11b interaction with the decapping coactivator Dcp1a, while preventing phosphorylation at S334 potentiates its interaction with the Ccr4-Not deadenylase complex subunit Cnot1. Collectively our findings establish for the first time that cAMP-elicited phosphorylation of TIS11b plays a key regulatory role in its mRNA decay-promoting function.**

Monitoring Editor
Marvin P. Wickens
University of Wisconsin

Received: Jun 7, 2016
Revised: Sep 29, 2016
Accepted: Sep 30, 2016

This article was published online ahead of print in MBoC in Press (http://www.molbiolcell.org/cgi/doi/10.1091/mbc.E16-06-0379) on October 5, 2016.

†These authors contributed equally to this work.

*Address correspondence to: Nadia Cherradi (nadia.cherradi@cea.fr).

Abbreviations used: ACTH, adrenocorticotropin; ARE, AU-rich element; BAC, bovine adrenocortical; BRF1, butyrate response factor 1; CHIP, chromatin immunoprecipitation; CI, confidence interval; CRE, cAMP response element; CTD, C-terminal; DRB, 5,6-dichloro-1-β-D-ribofuranosylbenzimidazole; IgG, immunoglobulin G; MAPK, MAP kinase; MK2, MAPK-activated protein kinase 2; NTD, N-terminal domain; OA, okadaic acid; PBS, phosphate-buffered saline; PKA, cAMP-dependent protein kinase; PKB, protein kinase B; PP2A, protein phosphatase 2A; RT-qPCR, quantitative reverse transcription-PCR; TIS11b, TPA-inducible sequence 11b; TSS, transcription start site; TTP, tristetraprolin; TTP-CIM, TTP-Ccr4-Not interaction motif; VEGF, vascular endothelial growth factor; WT, wild type.

INTRODUCTION

Besides transcription, posttranscriptional mechanisms play a major role in the regulation of gene expression. In particular, mRNA stability is a key step that progressively appears to be a highly regulated step. Importantly, this mechanism is responsive to modifications of the cellular environment (hormonal variations, hypoxia, etc.) and regulates the expression of subsets of proteins whose levels need to be rapidly adjusted. The regulation of mRNA stability involves *cis* sequences located mainly in the 3′ untranslated region (UTR) of the target mRNA that are bound by *trans*-acting factors. The most studied *cis* element is the AU-rich element (ARE) located in the 3′ UTR of short-lived mRNAs encoding proteins such as cytokines, growth factors, or metabolic regulators.

A great effort has been devoted over the past two decades to the identification of ARE-binding proteins and analysis of their contribution to the control of mRNA stability (Garneau *et al*., 2007). mRNA-stabilizing proteins include the members of the Hu

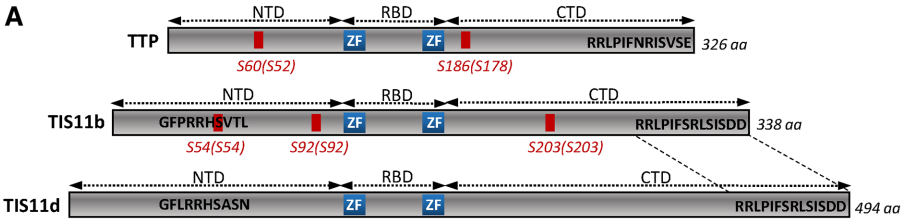

B

Family member	Kinase	Phosphorylation site	Effect on function	References
TIS11/TTP	MK2	S52, S178	Inhibition of mRNA decay, TTP protein stability	Chrestensen *et al.*, 2004; Stoecklin *et al.*, 2004; Clement *et al.*, 2011
TIS11b/BRF1	PKB	S92, S203	Inhibition of mRNA decay, BRF1 protein stability	Schmidlin *et al.*, 2004 Benjamin *et al.*, 2006
	MK2	S54, S92, S203	Inhibition of mRNA decay	Maitra *et al.*, 2008

FIGURE 1: Schematic representation of known phosphorylation sites in human TTP family members. (A) NTD and CTD represent the N-terminal and C-terminal activation domains on either sides of the zinc-finger (ZF) RNA-binding domain (RBD). The serines that have been shown previously to regulate TTP family function upon phosphorylation are indicated in red. Corresponding serines in mouse proteins are indicated with brackets. The conserved C-terminal sequence between TIS11b and TIS11d is indicated between dotted lines. Other phosphoserines have been identified in vitro and in phosphoproteomic studies of ectopically expressed TTP (reviewed in Venigalla and Turner, 2012). However, the relevance of these phosphosites remains to be validated experimentally. No phosphorylated serines in TIS11d/BRF2 have been reported so far. (B) Protein kinases regulating TTP family fate and function. aa, amino acid.

family (HuR, HuC, and HuD; Meisner and Filipowicz, 2010), whereas major mRNA-destabilizing proteins comprise members of the TIS11 family of double zinc-finger proteins, KSRP and AUF1 (Briata *et al.*, 2013; Brooks and Blackshear, 2013; White *et al.*, 2013). The TIS11 protein family is composed of four known members: TTP (Tristetraprolin/TIS11/ZFP36), TIS11b (ZFP36L1/BRF1), TIS11d (ZFP36L2/BRF2), and ZFP36L3, which is expressed exclusively in mouse placental tissue (Blackshear *et al.*, 2005). In vitro, the three main members of the TIS11 family (TTP, TIS11b, and TIS11d) have been shown to interact with several ARE-containing mRNAs and to trigger deadenylation and degradation of the target mRNAs (Baou *et al.*, 2009). However, genetic knockout of each member in mice leads to different phenotypes, thus suggesting that TIS11 proteins might have specific target mRNAs in vivo (Taylor *et al.*, 1996; Bell *et al.*, 2006; Stumpo *et al.*, 2009). TTP, the most-studied member of the TIS11 family, has been shown to trigger degradation of several transcripts, including TNF-α, GM-CSF, IL-2, and IL-10 mRNAs (Carballo *et al.*, 1998, 2000; Ogilvie *et al.*, 2005; Stoecklin *et al.*, 2008). TTP and TIS11b are able to recruit the components of the mRNA decay machinery (Fenger-Gron *et al.*, 2005; Lykke-Andersen and Wagner, 2005; Clement *et al.*, 2011). We have previously shown that TIS11b destabilizes the mRNA of the angiogenic cytokine vascular endothelial growth factor (VEGF; Ciais *et al.*, 2004) and the mRNA of the steroidogenic acute regulatory protein (Duan *et al.*, 2009) through interaction with ARE motifs in their 3′ UTRs. In endocrine cells, transient hormone-induced expression of VEGF mRNA is regulated through antagonistic actions of HuR and TIS11b (Cherradi *et al.*, 2006). More recently, we demonstrated that TIS11b controls mineralocorticoid receptor mRNA stability in renal cells exposed to hypertonicity in vitro and in vivo (Viengchareun *et al.*, 2014). Importantly, a cell-penetrating TIS11b exogenously delivered to preestablished tumors in mice exerts antiangiogenic and antitumoral effects through multitarget destabilization of tumor mRNAs (Planel *et al.*, 2010).

TIS11 family proteins are distal targets for signaling pathways, allowing transfer of external stimuli to the mRNA decay machinery (Venigalla and Turner, 2012). The p38 MAP kinase (MAPK) and its downstream kinase MAPK-activated protein kinase 2 (MK2) play a pivotal role in ARE-mediated mRNA decay. Activation of p38 MAPK has been shown to impair deadenylation of ARE-containing mRNAs, leading to mRNA stabilization (Marchese *et al.*, 2010). Macrophages from MK2$^{-/-}$ mice show severely reduced levels of TNFα, IL-1, IL-6, and IFNγ due to decreased cytokine mRNA stability (Kotlyarov *et al.*, 1999; Neininger *et al.*, 2002). A major target of MK2 is TTP, which is directly phosphorylated at Ser-52 (S52) and Ser-178 (S178) (Figure 1), allowing binding of 14-3-3 adaptor proteins (Chrestensen *et al.*, 2004). This interaction impairs the recruitment of the deadenylation machinery to the target mRNA (Stoecklin *et al.*, 2004; Clement *et al.*, 2011). On the other hand, phosphorylation of TTP by MK2 on S52 and S178 stabilizes TTP protein by preventing TTP degradation by the proteasome (Brook *et al.*, 2006). It has been suggested that MK2 is counterbalanced by protein phosphatase 2A (PP2A), which directly competes with 14-3-3 protein for binding to TTP. PP2A dephosphorylates TTP at Ser-178 (and possibly at other serine residues) and thereby activates mRNA decay (Sun *et al.*, 2007). More recently, phosphopeptide mapping and mass spectrometry analyses allowed the identification of a major tryptic phosphopeptide containing S90 and S93 in human TTP (Cao *et al.*, 2014).

In contrast with the accumulating data on the impact of TTP phosphorylation on its function, few studies address the role of TIS11b phosphorylation in ARE-mediated mRNA decay (Figure 1). Phosphorylation of TIS11b by the Akt/protein kinase B (PKB) at S92 and S203 abrogates mRNA decay of an IL-3 ARE-containing transcript and leads to TIS11b binding to 14-3-3 proteins and to TIS11b protein stabilization (Schmidlin *et al.*, 2004; Benjamin *et al.*, 2006). Phosphorylation of TIS11b by MK2 at S54, S92, and S203 inhibits its ability to destabilize ARE-containing mRNAs (Maitra *et al.*, 2008). The striking number of potential phosphorylation sites in the TIS11b sequence suggests that the protein has to integrate multiple signals to provide the appropriate cellular response. In this study, we show that the cAMP signaling pathway orchestrates all the steps controlling TIS11b expression and function, from TIS11b promoter activation to TIS11b protein phosphorylation. We identified two cAMP-dependent protein kinase (PKA) phosphorylation sites in living cells, S54 and S334, and investigated the role of these phosphosites in the control of TIS11b protein half-life and function in mRNA decay. Our data indicate that phosphorylation of S334 regulates the stability of TIS11b and its ability to interact with binding partners and to trigger mRNA degradation.

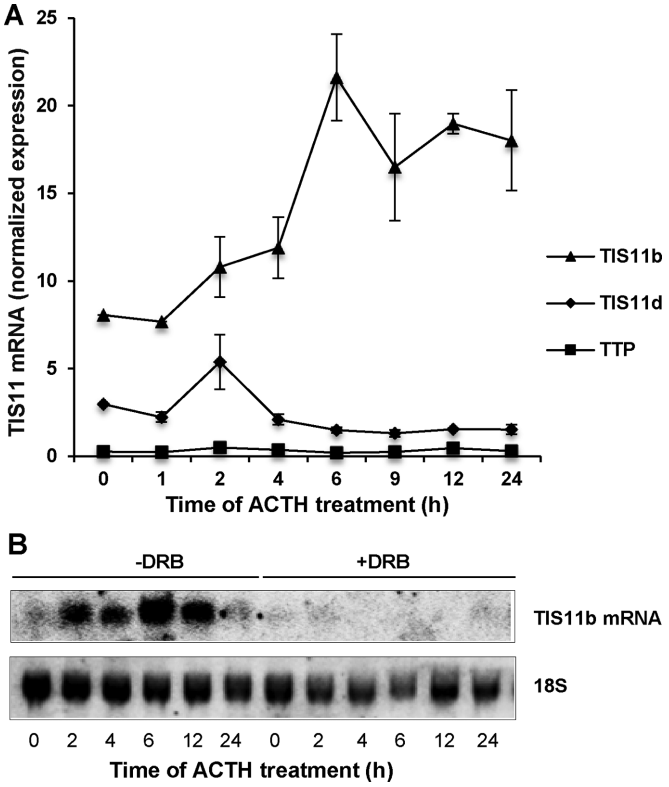

FIGURE 2: ACTH-induced expression of TIS11b mRNA in adrenocortical cells is transcription dependent. (A) Time-course analysis of TIS11 family member expression in BAC cells challenged with ACTH. RT-qPCR was performed as described in the Supplemental Material. Expression levels of TTP, TIS11b, and TIS11d mRNAs were normalized to RPL27 mRNA. Values are means ± SD of four independent experiments. (B) Northern blot analysis of TIS11b transcript levels in BAC cells challenged with ACTH in the absence or presence of the transcription inhibitor DRB. The membrane was hybridized to a radiolabeled TIS11b cDNA probe and rehybridized to 18S RNA probe for loading control. Shown is a representative Northern blot of six independent experiments.

RESULTS

The cAMP signaling pathway regulates TIS11b gene transcription through the binding of the cAMP-response element (CRE)-binding protein CREB to TIS11b promoter

In adrenocortical cells in primary culture, the TIS11b transcript is expressed at very low levels and is rapidly induced by the cAMP-mobilizing hormone adrenocorticotropin (ACTH; Chinn *et al.*, 2002; Cherradi *et al.*, 2006). For defining the mechanisms involved in TIS11b mRNA induction, bovine adrenocortical (BAC) cells were stimulated by ACTH in the presence of the transcription inhibitor 5,6-dichloro-1-β-D-ribofuranosylbenzimidazole (DRB). The hormone induced a marked increase in TIS11b mRNA levels, which was completely abrogated in the presence of DRB (Figure 2, A and B), thus suggesting a transcription-dependent mechanism. Interestingly, TTP or TIS11d mRNA levels were not significantly changed upon ACTH challenge, pointing at a specific induction of TIS11b by the hormone (Figure 2A). For testing potential promoter elements, up to 2000 nucleotides upstream of the transcription start site (TSS) of the TIS11b gene (*zfp36l1*) were inspected using Ensembl Genome Browser (www.ensembl.org) and the previously published partial promoter sequence of the rat TIS11b gene (*cMG1*) (Corps *et al.*, 1995). A TATAAA box and a cAMP response element (CRE) were found at –30 to –27 and at –402 to –394 relative to the TSS, respectively (Figure 3A). This sequence was highly conserved among species, suggesting an important role in cAMP-regulated TIS11b expression (Figure 3B). No classical CRE was identified within the –2000 base pairs upstream of the TSS of the two other family members TTP and TIS11d (unpublished data). A promoter sequence comprising the region –1038 to +52 relative to the TSS of human TIS11b was cloned and inserted in pGL3-luciferase reporter plasmid to study the activity of the canonical CRE (pWT construct; Figure 3C). Transfection of COS7 cells with pWT and subsequent treatment with forskolin to increase cAMP levels significantly stimulated the basal activity of the reporter gene about threefold, thus indicating that TIS11b promoter is regulated by the cAMP signaling pathway (Figure 3D). Cotreatment of COS7 cells with the cAMP-dependent protein kinase (PKA) inhibitor RpcAMP strongly inhibited the cAMP-induced activation of the reporter gene. To investigate the role of the putative CRE in mediating the response to cAMP, we mutated the CRE sequence TGACGTCA into TCTCGAGA (pmutCRE construct). Transfection of COS7 cells with pmutCRE completely abrogated forskolin-mediated stimulation of luciferase activity, thus indicating a key role of the CRE in cAMP-mediated transactivation of TIS11b promoter (Figure 3D). As the CRE-binding protein CREB functions as a *trans*-acting regulator of genes containing a CRE sequence in their promoter, we examined whether CREB was involved in transactivation of TIS11b promoter by cAMP using anti–phospho-CREB antibodies. Forskolin or ACTH triggered a time-dependent phosphorylation of CREB peaking at 30 min in COS7 and BAC cells, respectively (Supplemental Figure S1, A–D). To provide further evidence that the CRE is implicated in CREB binding to DNA upon cAMP stimulation, we performed chromatin immunoprecipitation (CHIP) experiments in COS7 cells transfected with pWT promoter construct. A specific interaction occurred in vivo between CREB and TIS11b promoter at the basal level, and this interaction was increased at 30 min posttreatment with forskolin (Supplemental Figure S1E). Similarly, CHIP experiments in BAC cells challenged with ACTH revealed that CREB was bound to endogenous TIS11b promoter at 30 min poststimulation (Supplemental Figure S1F). Collectively these data indicate that the PKA signaling pathway regulates TIS11b gene transcription through CREB activation.

The cAMP-dependent protein kinase regulates TIS11b expression and phosphorylation

We have previously shown that ACTH increases TIS11b protein expression and that silencing of TIS11b compromises VEGF mRNA decay in endocrine cells (Chinn *et al.*, 2002; Cherradi *et al.*, 2006). In addition, activation of the cAMP signaling pathway induced a broad series of 38–50 kDa TIS11b bands that collapsed into a single band after λ-phosphatase treatment, indicating that the slower-mobility species arose from phosphorylation events (Duan *et al.*, 2009). For investigation of the role of PKA in the hormonal induction of TIS11b and its target mRNA, BAC cells were stimulated by ACTH for various periods of time in the absence or presence of H89, a PKA-specific inhibitor. Western blot analysis of cell lysates showed that the hormone induced a marked time-dependent increase in TIS11b protein levels (Figure 4, A and B) that was accompanied by a shift toward high-molecular-weight species (Figure 4A; see dotted lane as a reference for migration). In contrast, the levels of the three major VEGF isoforms ($VEGF_{121}$, $VEGF_{165}$, and $VEGF_{189}$; Planel *et al.*, 2010) peaked at 2 h, then decreased toward basal levels (Figure 4, A and C). Quantitative PCR analysis of total RNA revealed a transient ACTH-induced increase in VEGF mRNA levels, consistent with

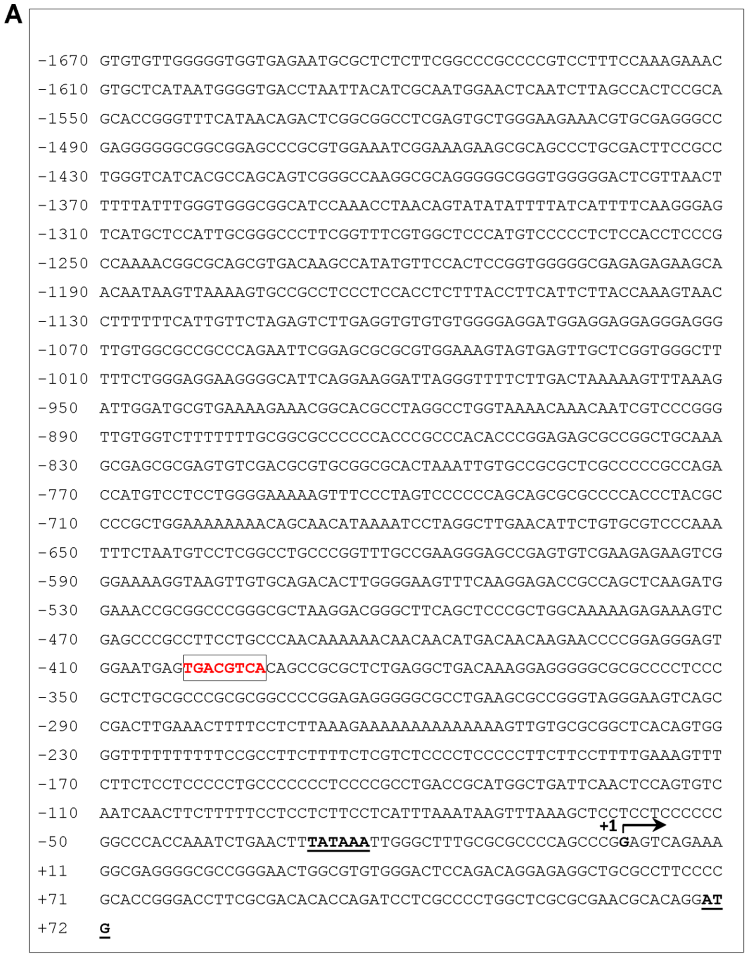

FIGURE 3: Cloning and analysis of TIS11b promoter. (A) The sequence of the human TIS11b promoter region from −1670 nucleotides upstream of the transcription start site (+1) to the translation initiation ATG was determined using Ensembl Genome Browser (www.ensembl.org). The CRE is shown in red, and the TATAA box (bold) is underlined. (B) The CRE in TIS11b promoter is conserved among species. (C) Schematic representations of TIS11b promoter region constructs. The WT construct contains 1088 base pairs of the promoter region. The mutCRE construct results from the substitution of four nucleotides within the CREB consensus sequence as described in the Supplemental Material. (D) WT and mutCRE constructs were inserted in pGL3-luciferase reporter plasmid and transfected in COS7 cells as described in the Supplemental Material. Promoter-driven luciferase activity was measured after cell stimulation with 25 μM forskolin in the presence or absence of RpcAMP (10 nM) for 24 h. Results are represented as a percentage of luciferase activity in control nonstimulated cells. Transfections were performed in triplicate, and values are means ± SD from three independent experiments. *, significantly different from pWT luciferase activity in control nonstimulated cells, with $p < 0.05$; #, significantly different from pWT luciferase activity in forskolin-treated cells, with $p < 0.05$.

VEGF protein expression (Figure 4D). Remarkably, the high induction of TIS11b at 6 h was correlated with low VEGF mRNA and protein levels. Stimulation of TIS11b and VEGF expression by ACTH were dramatically reduced in the presence of H89 (Figure 4, A–D) with disappearance of high-molecular-weight forms of TIS11b.

To further establish the effect of ACTH on TIS11b phosphorylation, we performed immunoprecipitation experiments in [^{32}P] orthophosphate-labeled BAC cells. A basal phosphorylation level of TIS11b was detected in control cells, while ACTH induced a robust and time-dependent increase of ^{32}P incorporation into TIS11b, which was markedly impaired in the presence of H89 (Figure 4E). Quantification of phospho-TIS11b/total TIS11b ratio in independent experiments revealed that ACTH increased TIS11b phosphorylation by 2.4 ± 0.4-fold at 6 h poststimulation (Figure 4F). We next performed in vitro phosphorylation experiments to determine whether TIS11b is a direct substrate of PKA. Purified recombinant glutathione *S*-transferase (GST)-TIS11b was incubated in the presence of the catalytic subunit of PKA and [γ-^{32}P]-labeled ATP. As shown in Figure 4G, TIS11b was efficiently phosphorylated by PKA in vitro. Taken together, these results suggest that activation of PKA signaling in endocrine cells is a pivotal mechanism whereby concomitant expression and phosphorylation of TIS11b are associated to a transient induction of its target mRNA VEGF.

Identification of PKA target sites within the TIS11b sequence: conserved S54 and S334 are phosphorylated in vitro and in vivo

TTP, TIS11b, and TIS11d each consist of an RNA-binding zinc-finger domain flanked by N-terminal (NTD) and C-terminal (CTD) domains that can activate mRNA decay (Figure 1; Lykke-Andersen and Wagner, 2005). Inspection of the coding sequence of TIS11b (SwissProt, accession number Q07352) using the Phosphorylation Site Predictor software DISPHOS 1.3 (www.dabi.temple.edu/disphos) revealed that the CTD of TIS11b harbors a majority of phosphorylatable serine residues as compared with the NTD (Supplemental Figure S2). By contrast, analysis of the TTP sequence showed that phosphorylatable serines were almost equally distributed between the NTD and the CTD of TTP. Interestingly, TIS11d displayed a similar profile of phosphorylatable serines in its distal CTD to that of TIS11b, while an

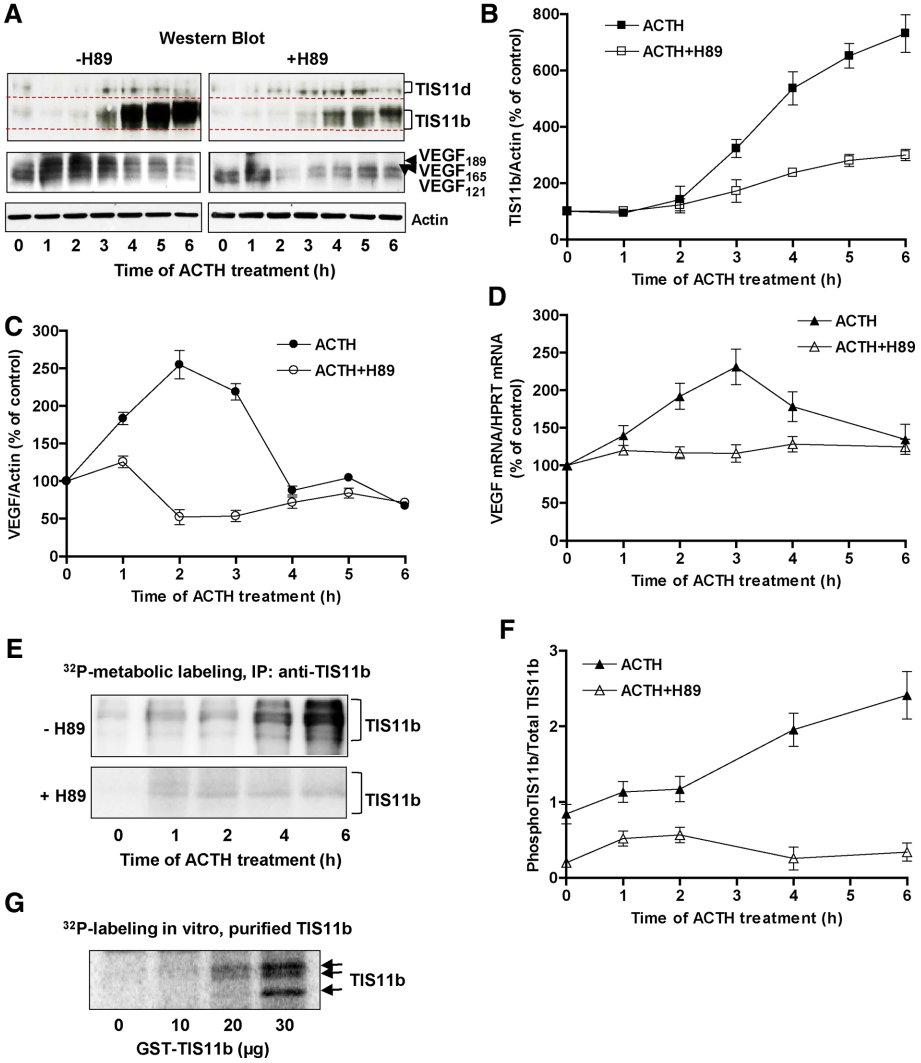

FIGURE 4: ACTH induces a cAMP-dependent expression and phosphorylation of TIS11b. (A) BAC cells were preincubated in the absence or presence of H89 (5 µM) for 30 min before addition of 10 nM of ACTH for the indicated periods of time. TIS11b and VEGF protein levels of whole-cell extracts (20 µg) were analyzed by Western blot. The blot was subsequently probed with an anti–β-actin to assess equal loading of samples. (B–D) Quantification of TIS11b, VEGF mRNA, and protein levels from independent experiments ($n = 5$, means ± SEM). Protein-level values were normalized to actin and are expressed as percentage of control values at time 0 (unstimulated cells). VEGF mRNA levels were measured by quantitative PCR and normalized to hypoxanthine-guanine phosphoribosyltransferase (HPRT). (E) Time-course of TIS11b phosphorylation in BAC cells stimulated with 10 nM of ACTH in the presence of [^{32}P]orthophosphate and in the presence or absence of H89. TIS11b was immunoprecipitated (IP) from cell extracts, resolved by SDS–PAGE, and then visualized by autoradiography. One representative experiment of four is shown. (F) Quantification of phospho-TIS11b/total TIS11b ratio in ACTH-stimulated BAC cells ($n = 4$, means ± SEM). (G) Phosphorylation of recombinant TIS11b by the catalytic subunit of PKA. Purified GST-TIS11b fusion protein was produced as described previously (Ciais *et al.*, 2004). Increasing doses of GST-TIS11b were subjected to in vitro phosphorylation as described in *Materials and Methods*. Protein extract from *Escherichia coli* (30 µg) transformed with empty pGEX vector was used as control in the phosphorylation assay (first lane, 0 µg).

additional phosphorylation hotspot was predicted close to TIS11d zinc-finger domain (Supplemental Figure S2). To identify putative PKA phosphorylation sites within TIS11b, we used the NetPhosK (www.cbs.dtu.dk/services/NetPhos) software. Four motifs corresponding to PKA consensus phosphorylation sites (RXS or RRXS), including S54, S92, S192, and S334 were found. As S54 and S334 presented the highest predictive score and as they were highly conserved not only between TIS11b and TIS11d but also between species (Figure 5A), we focused on both of these serines.

We first tested whether TIS11b peptides spanning either S54 (amino acids [aa] 50–60) or S334 (aa 330–338) were phosphorylated by PKA in vitro. SDS–PAGE analysis and autoradiography revealed a strong dose-dependent phosphorylation of the S54-bearing peptide, while PKA also phosphorylated the S334-bearing peptide, but to a lesser extent (Figure 5B). To determine whether S54 and S334 were directly targeted by PKA, we generated Flag-tagged wild-type (WT) and mutant TIS11b in which S54 or S334 was replaced by an alanine to prevent phosphorylation (S54A or S334A). Purified WT or mutant proteins were incubated in vitro with PKA. As shown in Figure 5, C and D, phosphorylation of TIS11b S54A or S334A mutants was significantly decreased as compared with the WT protein. These observations led us to investigate whether S54 and S334 were phosphorylated in vivo. We therefore generated phospho-S54–specific and phospho-S334–specific antibodies in rabbits immunized with phosphopeptides spanning S54 (CAGGGFPRRH(Sp)VTL) or S334 (RRLPIFSRL(Sp)ISD). The specificity of the sera was first evaluated by Western blot analysis of the phosphorylated and unphosphorylated control peptides (Figure 5E and Supplemental Figure S3). A site-specific and dose-dependent increase in phosphopeptide detection was observed, while the controls were not recognized by the phosphospecific antibodies. For further characterization of the phospho-S54–specific and phospho-S334–specific antibodies, phosphorylation of WT TIS11b or of the nonphosphorylatable TIS11b mutants (S54A or S334A) was monitored in COS7 cells transfected with pTarget-TIS11b constructs, then stimulated with forskolin in the absence or presence of H89 (Figure 5F). Endogenous TIS11b expression was barely detectable in COS7 cells (Figure 5F, empty pTarget plasmid or Vect). In basal conditions, a weak phosphorylation of endogenous TIS11b at S54 was detected, while the protein displayed three distinct forms phosphorylated at S334. These findings suggest that basal PKA activity in COS7 cells is sufficient for endogenous TIS11b phosphorylation. Forskolin-induced PKA activation led to a robust phosphorylation at both S54 and S334, which was prevented in the presence of H89. Importantly, the overexpressed TIS11b mutants S54A and S334A were not recognized by the phosphospecific antibodies (Figure 5F). These results indicate that the newly generated antibodies are phosphospecific and that the PKA-induced phosphorylation event is efficient on WT TIS11b but is not on the alanine substitution mutants.

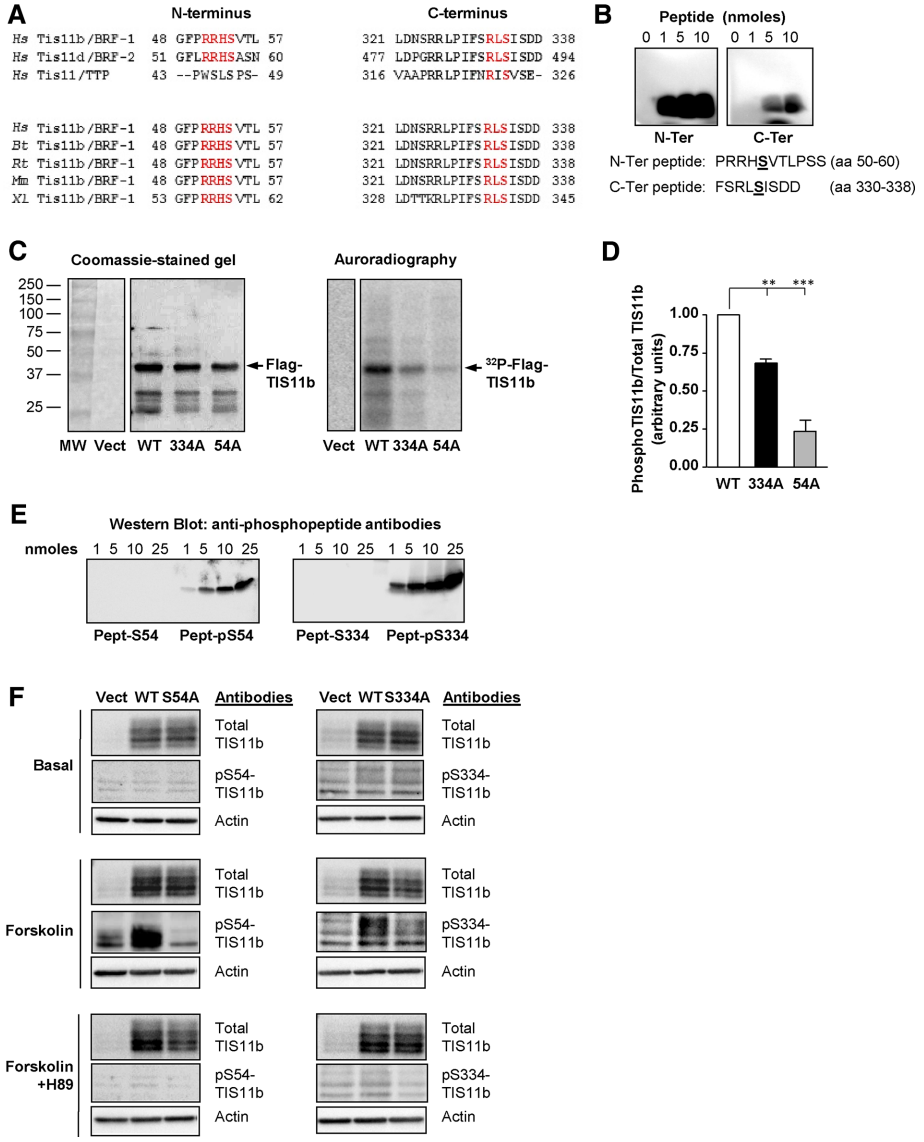

FIGURE 5: S54 and S334 are PKA target sites in vitro and in vivo. (A) Sequence alignment of conserved amino acid within the N-terminus and the C-terminus between TIS11b, TIS11d, and TTP showing PKA consensus motifs (highlighted in red, RRHS and RLS). These motifs are also conserved between species in TIS11b sequence and harbor S54 S334 (*hs*, *Homo sapiens*; *Bt*, *Bos taurus*; *Rt*, *Rattus norvegicus*; *mm*, *Mus musculus*; *xl*, *Xenopus laevis*). (B) Dose-dependent in vitro phosphorylation of synthetic N-terminal and C-terminal peptides of TIS11b by the catalytic subunit of PKA. Both peptides contain the PKA consensus motifs RRHS or RLS (S54 and S334 are shown in bold; aa, amino acids). Phosphorylated peptides were resolved by SDS–PAGE (15%) and visualized by autoradiography. (C) In vitro phosphorylation of recombinant Flag-WT TIS11b and Flag-TIS11b mutants S54A and S334A (1 μg purified proteins). Protein extracts from *E. coli* transformed with empty vector (pET15b) served as control (Vect). (D) PKA-mediated phosphorylation of recombinant TIS11b was significantly impaired when S54 and S334 were replaced by an alanine. Ratios of phosphorylated protein/total protein are reported ($n = 4$ independent experiments, mean ± SEM). Asterisks: significantly different from the WT with $^{**}p < 0.01$ and $^{***}p < 0.001$. (E) Characterization of the phosphospecific antibodies in vitro. Unphosphorylated control peptides were run alongside phosphorylated peptides to determine whether the antibodies could detect the phospho-S34 (pS54) or phospho-S334 (pS334). (F) Characterization of the phosphospecific antibodies in forskolin-stimulated cells. COS7 cells were transfected with empty pTarget Vector (Vect), pTarget-WT TIS11b (WT), pTarget-TIS11b-S54A, or pTarget-TIS11b-S334A plasmids and then stimulated or not (basal) with 25 μM of forskolin for 60 min in the presence or absence of H89. Cell lysates were analyzed by Western blot to assess the specificity of the anti-pS54 or anti-pS334 antibodies. Blots were imaged simultaneously with the Chemidoc Imaging system for 5 s to accurately detect strong and weak bands for all conditions.

TIS11b is phosphorylated at S54 and S334 in both endocrine and cancer cells

To assess whether TIS11b is phosphorylated at S54 and S334 in different cell types, we used the highly differentiated BAC cells and the human lung carcinoma cell line A549. BAC cells were challenged with ACTH for various periods of time (Figure 6A). Cell lysates were probed either with specific anti–total TIS11b/TIS11d (Chamboredon *et al.*, 2011) or with phosphospecific antibodies. It is worth mentioning that TIS11d expression was variable between primary cultures of BAC cells. TIS11d was detected at the basal level and slightly decreased at 6 h poststimulation, while TIS11b was nearly undetectable at the basal level and markedly up-regulated at 6 h by ACTH treatment. ACTH also increased the phospho-S54 signal, which paralleled the increase in total TIS11b protein levels. Interestingly, TIS11d was heavily labeled with the anti–phospho-S54 due to the conservation of the RRHS motif (S57 in TIS11d) between TIS11b and TIS11d. No phospho-S334 signal was detected for TIS11b before 6 h of stimulation by the hormone, suggesting a delayed ACTH-induced phosphorylation of this residue (Figure 6A). The single band detected belongs to the high-molecular-weight species of TIS11b (shown by an asterisk). As observed with the anti–phospho-S54, TIS11d was markedly labeled with the anti–phospho-S334 antibodies (S490 in TIS11d). Again, this result is likely due to the perfect conservation of the C-terminal peptide between TIS11b and TIS11d. Importantly, cotreatment of BAC cells with ACTH and the PKA inhibitor H89 abrogated TIS11b induction and TIS11b phosphorylation at S54 and S334 (Figure 6A).

We next evaluated whether phosphorylation of S54 and S334 could occur in another cellular context. Besides hormones, hypoxia is another regulator of TTP protein family expression (Sinha *et al.*, 2009; Kim *et al.*, 2010; Chamboredon *et al.*, 2011). In particular, TIS11b expression was shown to be increased in von Hippel–Lindau (VHL)-expressing renal cell carcinoma in response to hypoxia (Sinha *et al.*, 2009). A549 lung carcinoma cells were exposed to normoxia or hypoxia (1.5% O_2) for 2–8 h, then total cell extracts were analyzed by Western blot. A transient but robust increase in TIS11b levels was observed under hypoxia, peaking between 2 and 4 h of exposure and declining at 8 h (Figure 6B). This increase in total protein level was accompanied by an increase in the quantity of phosphorylated TIS11b at the S54 and S334 residues. Interestingly, as observed for TIS11b, TIS11d was

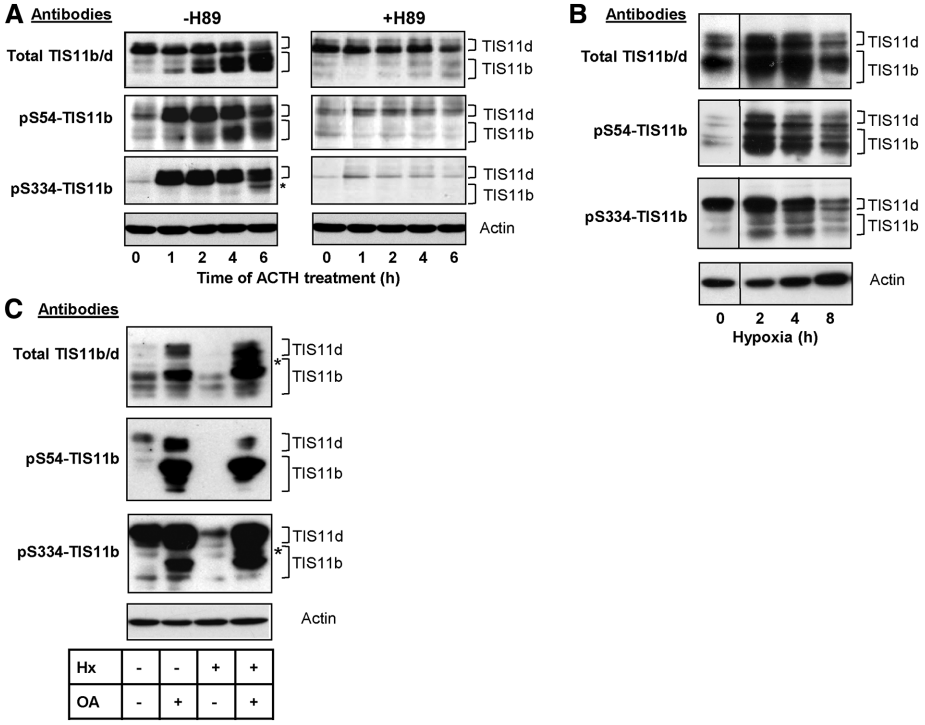

FIGURE 6: TIS11b is phosphorylated at S54 and S334 in hormone- and hypoxia-stimulated cells. (A) BAC cells were stimulated with ACTH in the presence or absence of H89 for the indicated periods of time. Total-cell extracts were probed for total TIS11b/TIS11d, pS54-TIS11b, and pS334-TIS11b. Owing to the conserved PKA consensus motifs (RRHS and RHS; see Figure 2) within TIS11b and TIS11d sequences, both phosphoproteins were detected. Note the shift of TIS11b toward high-molecular-weight species. The asterisk indicates the phospho-(S334)-TIS11b species appearing at 6 h poststimulation by ACTH. (B) A549 lung carcinoma cells were exposed to normoxia (0 h) or hypoxia for 2, 4, and 8 h. Cells extracts were probed by Western blot as described in A. (C) A549 cells were exposed to normoxia or hypoxia for 8 h in the absence or presence of OA, an inhibitor of the phosphatases PP2A/PP1. Note the pS334-TIS11b species appearing under hypoxia in the presence of OA (indicated by an asterisk). Blots were subsequently probed with an anti–β-actin to assess equal loading of samples.

heavily labeled with anti–phospho-S54-antibodies in response to hypoxia. By contrast, TIS11d was labeled with anti–phospho-S334-antibodies in both normoxic and hypoxic conditions.

As the phosphorylation status of the TIS11b protein family is under the dual control of kinases and phosphatases (Benjamin *et al.*, 2006; Brook *et al.*, 2006; Sun *et al.*, 2007), we sought to determine whether inhibition of serine/threonine phosphatases could impact the level of hypoxia-induced phosphorylation of S54 and S334 within TIS11b. Therefore A549 cells were exposed to normoxia or hypoxia for 8 h in the absence or presence of okadaic acid (OA), a potent inhibitor of protein phosphatases PP1 and PP2A. As shown in Figure 6C, treatment of A549 cells by OA markedly increased total TIS11b protein levels in normoxia, and this up-regulation was even more pronounced in response to hypoxia. In addition, OA induced accumulation of low-mobility bands of TIS11b under hypoxia (Figure 6C, top, asterisk). TIS11b protein was highly phosphorylated at S54 after OA treatment in normoxia and hypoxia (Figure 6C). Remarkably, OA-induced TIS11b was heavily phosphorylated at S334 under hypoxia with appearance of low-mobility forms of the protein (Figure 6C, bottom, asterisk). Altogether these results indicate that the S54 and S334 residues of TIS11b and their counterparts in TIS11d are phosphorylation target sites. Moreover, both residues were phosphorylated under different physiological conditions and in different cell types, suggesting that they may play a wide biological role in TIS11b function.

S54 and S334 are involved in the control of TIS11b protein half-life

TIS11b protein turnover was shown to be regulated by PKB through S92 and S203 phosphorylation sites (Benjamin *et al.*, 2006). We sought to investigate whether S54 and S334 were also involved in the regulation of TIS11b protein half-life. COS7 cells were transfected with WT TIS11b, TIS11b-S54A, TIS11b-S54D, TIS11b-S334A, or TIS11b-S334D mutants, and then translation was arrested by cycloheximide at the indicated time points. The steady-state levels of TIS11b alanine mutants (S54A and S334A) were lower than those of WT TIS11b (time point $t = 0$, Figure 7A), while the steady-state levels of TIS11b aspartate mutants (S54D and S334D) were higher than those of WT TIS11b. These results suggest that S54 and S334 substitutions impact TIS11b protein turnover. Nonlinear regression to a first-order exponential decay model yielded a half-life for WT TIS11b of 252.1 min (Figure 7, B and C). The mutant TIS11b-S54A displayed a shorter half-life of 141.5 min, while the half-life of the TIS11b-S54D mutant was higher than that of the WT ($t_{1/2}$ = 273.6 min). The TIS11b-S334A mutant was less stable ($t_{1/2}$ = 204.0 min) than WT TIS11b. By contrast, TIS11b protein stability was substantially increased when the S334 was replaced by the phosphomimetic aspartate (TIS11b-S334D), with a half-life of 413.8 min. Comparison of the best-fit values showed that the half-lives of TIS11b-S54A and TIS11b-S334D were the most significantly different from the half-life of WT TIS11b (Figure 7C). These data indicate that S54 and S334 are critical residues in the control of TIS11b turnover.

Mimicking phosphorylation at S334 potentiates TIS11b-mediated decrease in reporter mRNA activity and VEGF mRNA steady-state levels

TIS11b is a direct substrate of the kinases Akt/PKB (Schmidlin *et al.*, 2004; Benjamin *et al.*, 2006) and MK2 (Maitra *et al.*, 2008). PKB- and MK2-induced phosphorylations of TIS11b at Ser-90/Ser-92/Ser-203 were reported to inhibit TIS11b-mediated ARE mRNA decay (Schmidlin *et al.*, 2004; Stoecklin *et al.*, 2004; Benjamin *et al.*, 2006). For determining the role of S54 and S334 in TIS11b function, the mRNA-destabilizing activity of WT TIS11b, TIS11b-S54A, TIS11b-S54D, TIS11b-S334A, and TIS11b-S334D mutants was first assessed using a Luciferase-VEGF 3′ UTR fusion construct (Ciais *et al.*, 2004) whose activity is driven by the ARE-containing 3′ UTR of VEGF. To ensure that differences in reporter activity were not due to differences in TIS11b protein expression levels, we transfected variable doses (3–10 ng) of TIS11b constructs on the basis of half-life determinations (Figure 8) to achieve similar basal levels of TIS11b expression. As shown in Figure 8A, overexpression of WT TIS11b decreased luciferase activity by 43.4 ± 1.5%. Substitution of S54 by an alanine (S54A) modestly, although significantly, affected TIS11b-mediated decrease in luciferase activity (55.9 ± 1.0% inhibition). The

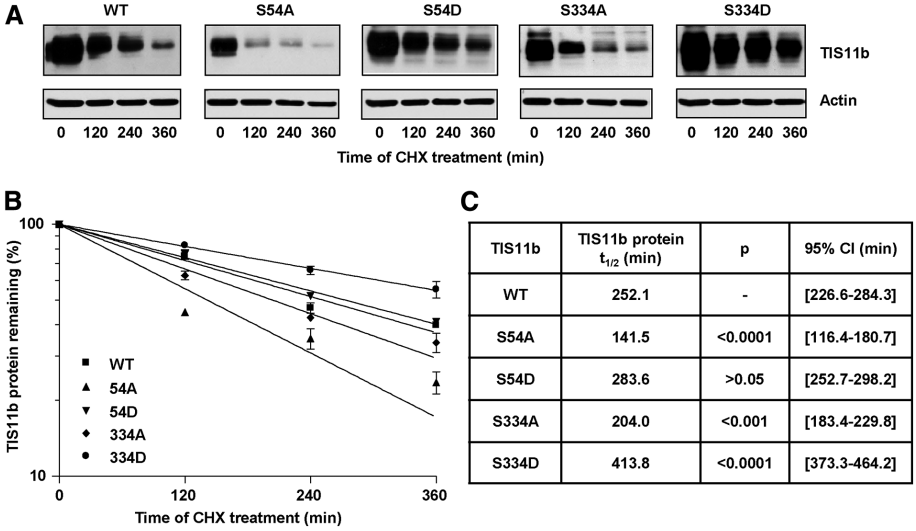

C

TIS11b	TIS11b protein $t_{1/2}$ (min)	p	95% CI (min)
WT	252.1	-	[226.6-284.3]
S54A	141.5	<0.0001	[116.4-180.7]
S54D	283.6	>0.05	[252.7-298.2]
S334A	204.0	<0.001	[183.4-229.8]
S334D	413.8	<0.0001	[373.3-464.2]

FIGURE 7: S54 and S334 regulate TIS11b protein stability. (A) COS7 cells were cotransfected with 10 ng of pTarget plasmids encoding WT TIS11b (WT), TIS11b S54A, TIS11b S54D, TIS11b S334A, or TIS11b S334D mutants and then treated with cycloheximide (CHX) as described in *Materials and Methods*. The half-life of WT or mutant TIS11b was analyzed by Western blot. All the membranes were exposed simultaneously for 15 s. Quantification of TIS11b steady-state levels (TIS11b/actin ratio) at $t = 0$ yielded the ratios 1, 0.61, 1.27, 0.85, and 1.58 for WT TIS11b, TIS11b-S54A, S54D, TIS11b-S334A, and TIS11b-S334D mutants, respectively. (B) TIS11b protein levels were normalized to actin levels and plotted as a percentage of the initial value against time using nonlinear regression to a first-order exponential decay model. (C) Calculated half-lives of TIS11b from four independent experiments. Half-lives of TIS11b mutants were compared with the half-life of WT TIS11b. *p* Values and 95% confidence intervals (CIs) were determined using an *F*-test.

activity of the mutant TIS11b-S54D was not statistically different from that of the WT. When S334 was replaced by an alanine (S334A), the inhibitory effect of TIS11b was significantly impaired (15.3 ± 3.2% inhibition). Replacing S334 by an aspartate (S334D) significantly potentiated the inhibitory effect of TIS11b on luciferase activity (65.2 ± 2.9% inhibition). Importantly, the observed differences in luciferase activities were not due to differences in expression levels of TIS11b (Figure 8A, bottom panel).

We next examined the effect of TIS11b mutant expression on endogenous VEGF mRNA steady-state levels. Overexpression of each mutant followed by Northern blot analysis revealed that the TIS11b-S54A mutant was slightly more active than the WT in decreasing VEGF mRNA, while TIS11b-S54D was less efficient (Figure 8, B–D). Remarkably, the mutant TIS11b-S334D was significantly more active than the WT, while the activity of TIS11b-S334A mutant was significantly impaired. Altogether these results suggest that phosphorylation at S54 leads to a modest impairment of TIS11b-elicited decrease in VEGF transcript, whereas phosphorylation at S334 potentiates TIS11b function.

Mimicking phosphorylation at S334 enhances TIS11b-elicited VEGF mRNA decay

We next examined the effect of TIS11b mutant expression on endogenous VEGF mRNA turnover (Figure 9). COS7 cells were transfected either with WT or mutant TIS11b constructs and then treated with DRB for mRNA decay analysis (Figure 9A). Nonlinear regression to a first-order exponential decay model yielded a half-life of 177.5 min for VEGF mRNA in cells transfected with the empty vector (Figure 9, B and C). Overexpression of WT TIS11b significantly decreased VEGF mRNA half-life to 71.5 min, while the TIS11b-S54A mutant modestly affected VEGF mRNA decay ($t_{1/2}$ = 63.8 min). The TIS11b-S334A mutant was significantly less active than WT TIS11b in promoting VEGF mRNA decay ($t_{1/2}$ = 95.5 min). By contrast, we observed that VEGF mRNA decay was markedly accelerated by the TIS11b-S334D mutant when compared with WT TIS11b ($t_{1/2}$ = 40.6 min). Comparison of the best-fit values showed that TIS11b-S334D–elicited mRNA decay was highly significantly different from WT TIS11b–elicited mRNA decay (Figure 9C). These results suggest that mimicking phosphorylation at the residue S334 enhances the mRNA-destabilizing function of TIS11b.

S334 is a key residue in TIS11b interaction with the mRNA decay machinery

TTP has been reported to activate both 3′→5′ mRNA decay, by recruiting the multisubunit Ccr4-Not deadenylase complex to the mRNA, and 5′→3′ mRNA decay, by recruiting the decapping enzymes Dcp2/Dcp1a and the exonuclease Xrn1 (Fenger-Gron *et al.*, 2005; Lykke-Andersen and Wagner, 2005; Marchese *et al.*, 2010; Clement *et al.*, 2011; Sandler *et al.*, 2011; Fabian *et al.*, 2013). The Ccr4-Not complex comprises several proteins named Ccr4-Not (Cnot) subunits. The Cnot1 subunit is a scaffold for the other Ccr4-Not components, including Ccr4 and Caf1 deadenylases (Goldstrohm and Wickens, 2008). While some studies have shown that the Ccr4-Not complex interacts with the NTD of TTP (Lykke-Andersen and Wagner, 2005), more recent data pointed at interactions of the complex with the CTD of TTP (Sandler *et al.*, 2011; Fabian *et al.*, 2013). A crystal structure of Cnot1, a core subunit of Ccr4-Not, associated with a C-terminal peptide of TTP, led to the identification of a TTP-Ccr4-Not interaction motif (TTP-CIM; Figure 10A; Fabian *et al.*, 2013). TTP-CIM is highly conserved between TTP family members and comprises the S323 residue in TTP that corresponds to the S334 residue in TIS11b. To understand the functional effects of the phosphomimetic TIS11b-S334D mutant, we examined protein–protein interactions between WT TIS11b or its S334 mutants and components of the mRNA decay machinery. As it was technically challenging to detect some of the mRNA decay enzymes in COS7 cells, coimmunoprecipitation experiments were performed using HEK 293T cells transfected with WT TIS11b, TIS11b-S334A, or TIS11b-S334D mutant expression plasmids. TIS11b was subsequently immunoprecipitated from cell extracts, and the amounts of Cnot1, Dcp2, Dcp1a, or Xrn1 in the immunoprecipitates were detected by immunoblotting. Figure 10B shows that WT and mutant TIS11b were expressed at similar levels in transfected cells (input panel) and immunoprecipitated equally efficiently from cell extracts (IP panel). Protein complexes immunoprecipitated by anti-TIS11b antibodies contained Cnot1, Dcp2, Dcp1a, and Xrn1 but not HuR (negative control; Figure 10B), an ARE-binding protein that is not an activator of mRNA decay (Fan and Steitz, 1998). This result indicates that WT TIS11b exists in a complex with the major mRNA decay proteins. The nonphosphorylatable mutant TIS11b-S334A showed an increased interaction with Cnot1 as compared with that observed with the phosphomimetic mutant TIS11b-334D (Figure 10, B and C).

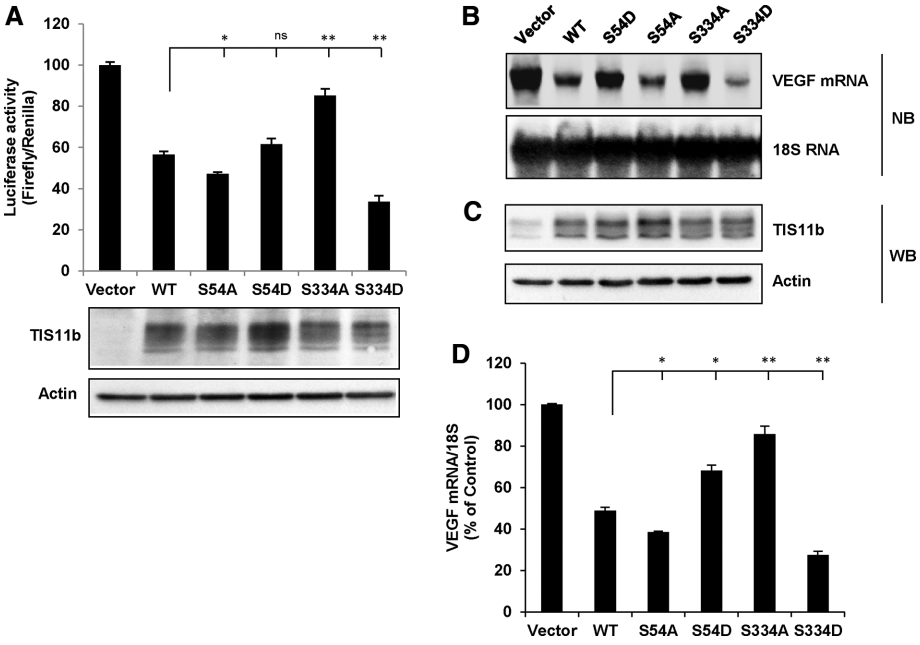

FIGURE 8: The phosphomimetic TIS11b-S334D mutant is more potent than WT TIS11b in decreasing VEGF 3′ UTR–driven luciferase activity and endogenous VEGF mRNA steady-state levels. (A) COS7 cells were cotransfected with pLuc 3′ UTR and pTarget plasmids encoding WT TIS11b, TIS11b-S54A, TIS11b-S54D, TIS11b-S334A, or TIS11b-S334D mutants. Firefly/*Renilla* luciferase activities of cell lysates were measured as described in *Materials and Methods*. Results are expressed as relative light units of firefly luciferase activity over relative light units of *Renilla* luciferase activity and are represented as a percentage of the luciferase activity in control cells transfected with empty pTarget plasmid. Transfections were performed in triplicate, and values are means ± SEM from seven independent experiments. The lower panel is a representative Western blot analysis of overexpressed TIS11b proteins showing that equivalent amounts of overexpressed TIS11b were recovered. (B) Northern blot (NB) analysis of endogenous VEGF mRNA in COS7 cells transfected as in A. (C) Western blot (WB) analysis of TIS11b protein expression levels in the COS7 cells used for the Northern experiment shown in B. (D) Quantification of VEGF mRNA steady-state levels in four independent experiments (means ± SEM). Asterisks: significantly different from WT with $*p < 0.05$ and $**p < 0.01$ (one-way ANOVA).

These findings suggest that S334 is a regulatory residue in TIS11b-mediated recruitment of the Ccr4-Not complex and that phosphorylation at this site might impair TIS11b and Ccr4-Not interaction. Therefore it is unlikely that the observed potentiated activity of TIS11b-S334D mutant on mRNA decay results from an enhanced recruitment of the deadenylase complex at the CTD of TIS11b. We thus investigated the impact of S334 substitutions on TIS11b interaction with the 5′→3′ mRNA decay machinery proteins. Figure 10B shows that Xrn1, Dcp1a, and Dcp2 coprecipitated with TIS11b. No differences were observed in immunoprecipitated levels of Xrn1 or Dcp2 in the presence of WT TIS11b or its mutants S334A and S334D. By contrast, the S334D mutant coprecipitated with a greater amount of Dcp1a than did the S334A nonphosphorylatable mutant. Together these results suggest that mimicking phosphorylation at S334 in the CTD of TIS11b stimulates its interaction with the decapping cofactor Dcp1a and that the phosphorylation status of TIS11b at the S334 site could modulate decapping efficiency.

DISCUSSION

TIS11 proteins are targets of several protein kinases that modulate their mRNA-decay promoting activity and their protein stability (Baou *et al.*, 2009; Brooks and Blackshear, 2013). In this report, we provide the first evidence that TIS11b transcription, expression, and phosphorylation are under the control of the cAMP signaling pathway. We uncovered novel PKA-dependent phosphorylations of the NTD and CTD of TIS11b in vitro and in vivo and identified S54 and S334 as physiological phosphorylation sites of PKA. Our major findings suggest that phosphorylation at S334 markedly enhances TIS11b protein stability and TIS11b association with the decapping coactivator Dcp1a. Both events might contribute to the increased efficiency of phospho–S334-TIS11b to trigger mRNA turnover.

We have previously shown that ACTH induces a transient increase in VEGF mRNA levels and that TIS11b is involved in the decay phase of VEGF mRNA expression (Chinn *et al.*, 2002; Cherradi *et al.*, 2006). The present study indicates that the hormone also induces a rapid phosphorylation of TIS11b that is significantly blunted upon inhibition of PKA. Because the NTD and CTD of TIS11 proteins family have been suggested to play different roles in the recruitment of the mRNA decay machinery (Lykke-Andersen and Wagner, 2005; Sandler *et al.*, 2011), we studied the most distal serines in the NTD and CTD that were predicted as target residues for PKA, namely S54 and S334. Using peptide fragments containing S54 or S334 residues, we found that these sites are indeed phosphorylated by PKA in vitro. Substitution of S54 or S334 by an alanine in recombinant proteins impaired PKA-mediated phosphorylation, thus confirming that they are PKA target sites. Interestingly, S54 has been reported previously as a target of MK2 in vitro in conjunction with S92 and S203 (Maitra *et al.*, 2008). The similarity between MK2 and PKA consensus phosphorylation sites (RXXS and RRXS, respectively) could result in shared serine targets. Nevertheless, the role of S54 or S334 alone in the regulation of TIS11b-dependent mRNA decay has not been investigated. Our finding that S54 and S334 are phosphorylated not only in a hormonally regulated cellular context but also during cancer cell response to hypoxic stress suggests that both serines are important regulatory phosphosites in TIS11b-dependent mRNA decay. Remarkably, PKA-dependent phosphorylation at S334 occurs in the late phase of TIS11b induction by ACTH, which is associated with decreased levels of VEGF mRNA. In this context, we hypothesized that S334 phosphorylation contributes to the destabilization of VEGF mRNA by TIS11b. The kinase involved in the phosphorylation of S54 and S334 in response to hypoxia remains to be identified. A study reporting the mammalian target of rapamycin–regulated phosphoproteome identified S334 as a target residue in TIS11b (Hsu *et al.*, 2011). Our observation that inhibition of phosphatase PP2A by OA increases the phosphorylation of both serines is in line with previous studies showing that PP2A inhibition increases TTP phosphorylation in macrophages (Sun *et al.*, 2007). The phosphorylation status of TIS11 proteins thus depends on a dynamic equilibrium between kinase and phosphatase activities.

Phosphorylation of TIS11b by Akt/PKB at S92 and S203 abrogates mRNA decay of an IL-3 ARE-containing probe and leads to TIS11b binding to 14-3-3 proteins and to TIS11b protein stabilization

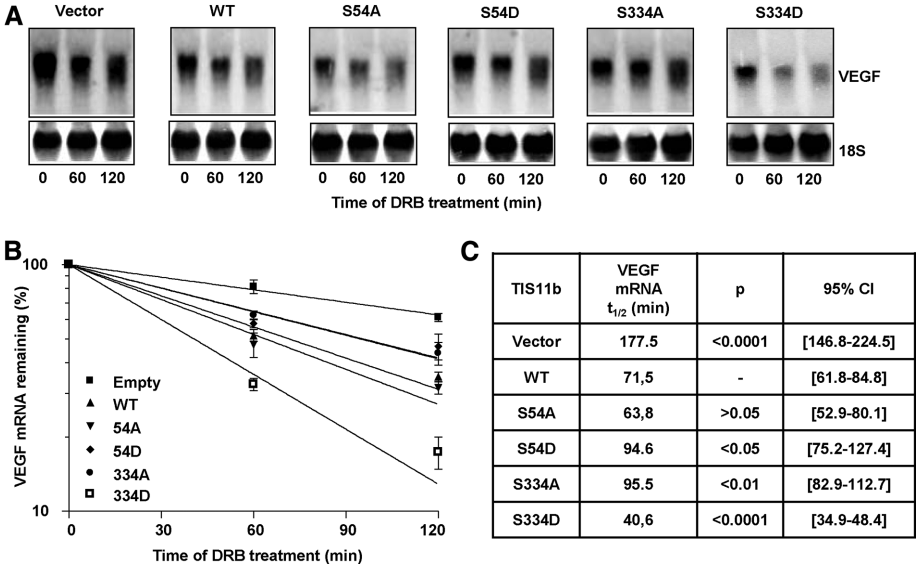

C

TIS11b	VEGF mRNA $t_{1/2}$ (min)	p	95% CI
Vector	177.5	<0.0001	[146.8-224.5]
WT	71,5	-	[61.8-84.8]
S54A	63,8	>0.05	[52.9-80.1]
S54D	94.6	<0.05	[75.2-127.4]
S334A	95.5	<0.01	[82.9-112.7]
S334D	40,6	<0.0001	[34.9-48.4]

FIGURE 9: VEGF mRNA is more efficiently destabilized by the phosphomimetic TIS11b S334D mutant. (A) COS7 cells were transfected in 12-well plates with pTarget empty plasmid (Vector) or plasmids encoding WT or mutant TIS11b. AT 48 h after transfection, the transcription inhibitor DRB (10 µg/ml) was added, and total RNA was extracted at the indicated time points and analyzed by Northern blot. The membrane was hybridized to a radiolabeled VEGF 3′ UTR probe and rehybridized to 18S RNA probe for loading control. (B) VEGF mRNA levels were normalized to 18s RNA levels and plotted as a percentage of the initial value against time using nonlinear regression to a first-order exponential decay model. Shown are the mRNA decay rates from three pooled independent experiments. (C) VEGF mRNA half-lives were calculated and compared with the half-life of the transcript in the presence of WT TIS11b. *p* Values and 95% CIs were determined using an *F*-test.

(Schmidlin *et al.*, 2004; Benjamin *et al.*, 2006). We therefore tested the impact of S54 and S334 mutations on TIS11b protein turnover. We found a half-life of 4 h for WT TIS11b, whereas the mutant TIS11b-S54A was highly unstable compared with the WT ($t_{1/2}$ ~ 2 h). Notably, the phosphomimetic mutant TIS11b-S334D displayed a markedly enhanced stability ($t_{1/2}$ ~ 7 h) when compared with WT TIS11b, suggesting that the S334D mutation could favor a long-lasting action of the protein in mRNA decay.

Using in vitro kinase assays, Maitra *et al.* (2008) reported that phosphorylation of TIS11b by MK2 at S54, S92, and S203 did not affect its ability to bind to ARE or to recruit mRNA degradation enzymes but did nonetheless inhibit its ability to destabilize ARE-containing mRNA. In this study, we found that substitution of S54 alone by an alanine has a modest effect on VEGF mRNA turnover. This result suggests that phosphorylation of additional PKA target residues is needed to significantly alter TIS11b function. A potential candidate serine is S92, which was identified as a target of both PKA (our in silico prediction analysis) and MK2 (Maitra *et al.*, 2008). By contrast, we show for the first time that substitution of S334 by an alanine impairs TIS11b function in VEGF 3′ UTR–driven reporter assays and mRNA decay. Strikingly, the mutant TIS11b-S334D even proved to be more active than WT TIS11b in triggering VEGF mRNA degradation. Given the huge number of phosphorylatable serines in TIS11b (49 out of 338 amino acids), in particular in the CTD of the protein (Supplemental Figure S2), we hypothesized that TIS11b function in ARE-mediated mRNA decay could be modulated by antagonistic phosphorylation events that allow recruitment of different binding partners.

As TTP and TIS11b bind to ARE-containing mRNAs and function by recruiting mRNA decay enzymes onto the mRNAs, we investigated whether mimicking phosphorylation at S334 could impact TIS11b association with endogenous mRNA decay proteins. Recruitment of the Ccr4-Not deadenylase complex by TTP is emerging as a key mechanism in the initiation of ARE-mediated mRNA decay (Clement *et al.*, 2011; Sandler *et al.*, 2011; Fabian *et al.*, 2013). Very interestingly, Fabian *et al.* (2013) identified Ser-323 (homologous to S334 in TIS11b) in the CTD of TTP as a critical serine for its interaction with Cnot1. Structural analyses revealed that hydrogen bonding between Tyr-900 of Cnot1 and S323 of TTP contributes to a stable closed-loop conformation of TTP-CIM. Moreover, it was shown that a TTP-CIM peptide containing a phospho-S323 binds with a lower affinity to Cnot1 as compared with WT. Our study demonstrates for the first time that TIS11b also exists in a complex with endogenous Cnot1. Coimmunoprecipitation experiments show that replacing S334 by an alanine, thus preventing phosphorylation at this residue, potentiates the association of TIS11b with Cnot1. This observation thus supports the hypothesis of Fabian *et al.* (2013) suggesting that phosphorylation at S323 in TTP or at S334 in TIS11b would impair deadenylase recruitment to TTP or TIS11b. Nevertheless, the enhanced interaction that we found between the TIS11b-S334A mutant and Cnot1 was paradoxical with respect to the low activity of this mutant in reporter and mRNA decay experiments. These observations suggest that preventing phosphorylation of S334 alone is not sufficient to promote deadenylation. An alternative explanation could be that substitution of S334 alone by an alanine induces conformational changes of the C-terminus of TIS11b, which is not compatible with optimal recruitment of the deadenylases Caf1 and Ccr4 to TIS11b/Cnot1.

In contrast to TIS11b-S334A, we found that the phosphomimetic TIS11b-S334D was more active in decreasing VEGF mRNA half-life when compared with WT TIS11b, even though this mutant was not significantly different from WT TIS11b in its ability to associate with Cnot1. These results led us to evaluate whether recruitment to TIS11b of the 5′→3′ mRNA decay regulators, namely the Dcp2/Dcp1a decapping complex and the exonuclease Xrn1, was increased upon phosphorylation of S334. Yeast Dcp2, which has decapping activity, directly interacts with Dcp1a, which modulates its function. However, the human Dcp1a-Dcp2 interaction is believed to require additional cofactors (Lsm1-7, enhancers of decapping Edc3 and Edc4, and the RNA helicase RCK; van Dijk *et al.*, 2002; Fenger-Gron *et al.*, 2005; She *et al.*, 2008). Dcp1a not only accelerates the catalytic step of decapping, but it also links other decapping activators to Dcp2 (She *et al.*, 2008). Ectopically expressed TTP and TIS11b were shown to coprecipitate with Dcp1a and Dcp2 (Lykke-Andersen and Wagner, 2005). In addition, the NTD of TTP, but not the CTD, was found to associate with overexpressed Dcp2 and Dcp1a (Fenger-Gron *et al.*, 2005; Lykke-Andersen and Wagner, 2005). The interactions of the NTD and CTD of TIS11b with the decapping complex have not been tested in these studies. Nonetheless, the CTD of TIS11b was

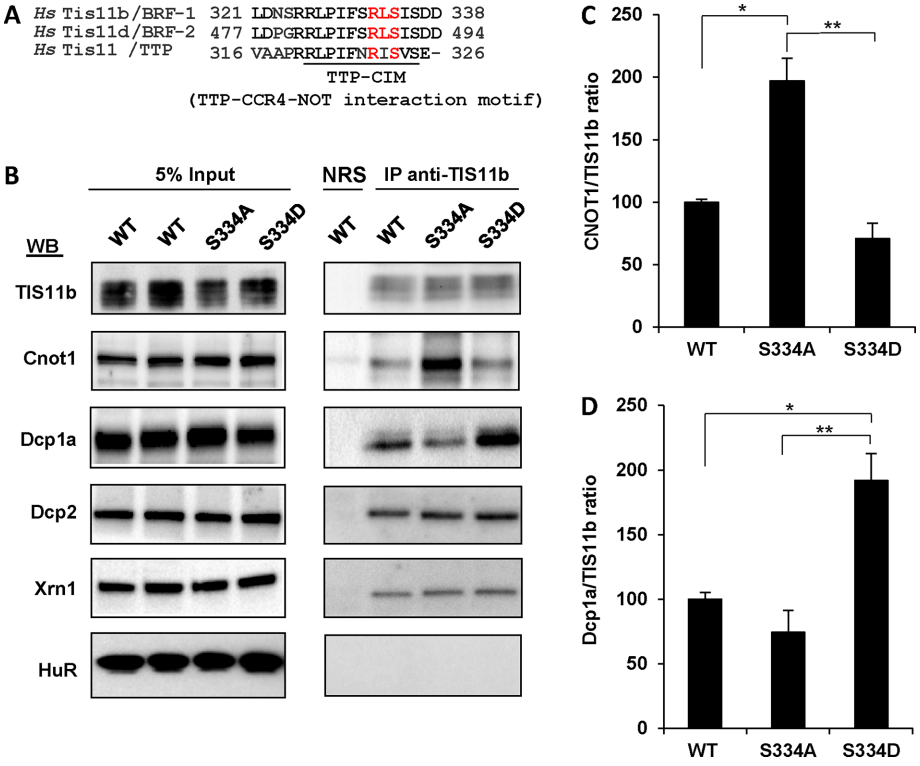

FIGURE 10: TIS11b S334D mutant exhibits enhanced interaction with the decapping complex activator Dcp1a. (A) Sequence alignment of the distal C-terminus of TTP family members, showing that the TTP-CCR4-NOT interaction motif is highly conserved between TTP family members (Fabian *et al.*, 2013). (B) Western blots showing association of TIS11b proteins with endogenous mRNA decay enzymes. Transiently expressed WT or TIS11b mutants were immunoprecipitated from HEK 293T cell extracts, and precipitates were probed for the presence of TIS11b and mRNA decay proteins. The mRNA-stabilizing protein HuR served as negative control and was not associated with TIS11b. NRS: immunoprecipitation reaction using normal rabbit serum in place of TIS11b antibodies. Input: 5% total-cell extract. (C, D) Quantification of Cnot1/TIS11b and Dcp1a/TIS11b ratio in three independent immunoprecipitation experiments. *, Significantly different from WT TIS11b with $p < 0.05$; **, significantly different from S334A mutant with $p < 0.01$ (one-way ANOVA).

found to be more active than the NTD in "tethered" mRNA decay (Lykke-Andersen and Wagner, 2005). In agreement with previous work, our results show that TIS11b is indeed associated with Dcp1a, Dcp2, and the 5′→3′exonuclease Xrn1 (Lykke-Andersen and Wagner, 2005). No difference was observed in TIS11b-S334A or TIS11b-S334D mutant interactions with Dcp2 and Xrn1. In contrast, we found that mimicking phosphorylation at S334 significantly enhanced TIS11b association with Dcp1a. These data suggest that the CTD of TIS11b, through the phosphorylation of this distal serine, could modulate TIS11b/Dcp1a interaction. Whether phosphorylation of S334 in TIS11b enhances the assembly and the efficiency of the decapping complex Dcp1a/Dcp2 remains to be determined in future studies.

A key finding of this study is that phosphorylation of TIS11b/BRF1 at a specific site is associated with activation of its function in mRNA decay. Our hypothesis is that cell signaling networks lead to changes in the phosphorylation status of TIS11b/BRF1 and other mRNA stability regulators, changing its interacting partners and thereby modifying the composition of the multimolecular complex targeting the mRNA. Remarkably, TTP is still efficient in promoting decay of TNFα mRNA following several hours of lipopolysaccharide (LPS) stimulation, during which the TTP protein is fully induced and phosphorylated (Carballo *et al.*, 1998). Maximal expression and phosphorylation of TIS11b is correlated with the lowest VEGF mRNA levels in endocrine cells. These observations suggest that combinatorial phosphorylations of TTP or TIS11b on specific residues, at least in some physiological situations, do not abrogate their mRNA destabilizing capability but rather fine-tune their interactions with the mRNA decay machineries.

MATERIALS AND METHODS

Cell culture

BAC cells were prepared by enzymatic dispersion of adrenal zona fasciculata-reticularis with trypsin, and primary cultures were established as previously described in detail elsewhere (Duperray and Chambaz, 1980). On day 4, 3×10^6 cells/10 cm-Petri dish were stimulated with 10 nM ACTH for the indicated periods of time in the presence or absence of the PKA inhibitor H89 (5 μM; Sigma-Aldrich, Saint-Quentin Fallavier, France). A549 cells were purchased from ATCC and cultured in DMEM GlutaMAX high glucose (Thermo Fisher, Saint Aubin, France) containing 10% fetal bovine serum (GE Healthcare, Velizy-Villacoublay, France) and 100 U/ml penicillin, 100 μg/ml streptomycin, and 30 μg/ml gentamicin. A549 cells (7.5×10^5) were seeded in 35 mm Petri dishes. One day later, they were exposed to hypoxia (1.5% O_2) in a hypoxia workstation (Don Whitley Scientific, H135, Shipley, UK) and harvested at the indicated time points for Western blot analyses. Alternatively, A549 cells were treated with 100 nM OA or dimethyl sulfoxide (Sigma-Aldrich) and then incubated under hypoxia. COS7 cells and HEK 293T cells were cultured as previously described (Planel *et al.*, 2010). All cell types were grown at 37°C in a 5% CO_2–95% air atmosphere.

Cloning and analysis of TIS11b promoter regulation by cAMP

Details are provided in the Supplemental Material.

Quantitative reverse transcription-polymerase chain reaction (RT-qPCR)

Details are provided in the Supplemental Material.

Plasmids

The plasmids pTarget-TIS11b-S54A, pTarget-TIS11b-S54D, pTarget-TIS11b-S334A, and pTarget-TIS11b-S334D were generated from pTarget-WT TIS11b (Ciais *et al.*, 2004) by site-directed mutagenesis (QuikChange XL site-directed mutagenesis kit; Agilent Technologies, Massy, France), using the primers indicated in Supplemental Table S1. For recombinant TIS11b, the constructs used were pET15b-Flag-TIS11b-S54A and pET15b-Flag-TIS11b-S334A, which were constructed as previously described for pET15b-Flag-TIS11b (Planel *et al.*, 2010), using their respective pTarget plasmids. Recombinant proteins were purified as previously described

(Planel *et al.*, 2010). All constructs were verified by sequencing (GATC Biotech, Mulhouse, France).

Transient transfections and dual luciferase activity assay

COS7 cells (1.5×10^5) were seeded in triplicate into 12-well plates and transfected on the following day using Lipofectamine (Thermo Fisher) according to the manufacturer's recommendations. pTarget-TIS11b plasmids (10 ng) were transfected in the presence of 500 ng of pLuc-VEGF 3′ UTR, and 25 ng of pRL-TK (Promega, Charbonnières, France) to compensate for variations in transfection efficiency (Planel *et al.*, 2010). *Renilla* and firefly luciferase activities were measured sequentially 24 h after transfection using the Dual-Luciferase reporter assay system (Promega) on a LUMAT LB 9507 luminometer (EGG-Berthold, Bad Wildbad, Germany). Results are expressed as relative light units of firefly luciferase activity over relative light units of *Renilla* luciferase activity and are represented as a percentage of the luciferase activity in control cells. Each transfection condition was performed in triplicate.

Metabolic labeling

BAC cells (5×10^6 cells/10 cm Petri dish) were prelabeled for 60 min in phosphate-free Ham's F12 medium containing 200 μCi/ml [^{32}P] orthophosphate, before exposure to 10 nM ACTH in the presence or absence of 10 μM H89 for the indicated time, at 37°C. At the end of the stimulation period, cells were washed twice with ice-cold phosphate-buffered saline (PBS) and lysed in 0.5 ml ice-cold RIPA lysis buffer containing a protease inhibitor cocktail, 5 mM sodium fluoride, 100 nM OA, and 200 μM sodium orthovanadate (Sigma-Aldrich). Samples were briefly centrifuged at $10{,}000 \times g$ for 15 min. Total cell lysates were precleared with 20 μl of protein A/G-agarose mixture and incubated with 1 μg/ml of rabbit polyclonal antibodies against the N-terminal and C-terminal peptides of TIS11b (Planel *et al.*, 2010) at 4°C for 12 h. The immune complex was isolated by adding 30 μl of protein A/G-agarose mixture for 2 h at 4°C and then centrifuging at 2000 rpm for 5 min. The pellet was washed four times with RIPA buffer and analyzed by SDS–PAGE and autoradiography.

In vitro phosphorylation

Recombinant GST-TIS11b (Ciais *et al.*, 2004), Flag-TIS11b, Flag-TIS11b-S54A, Flag-TIS11b-S334A, or synthetic peptides were incubated with the catalytic subunit of PKA (1 μg) in the presence of [γ-^{32}P]ATP (10 μCi), 0.2 mM of cold ATP, and 15 mM of $MgCl_2$ in Tris-HCl 50 mM (pH 7.4) for 20 min at 30°C in a final volume of 50 μl. Phosphorylation was stopped by the addition of 10 mM EDTA. The samples were analyzed by SDS–PAGE, and phosphoproteins or phosphopeptides were visualized by autoradiography.

Generation of TIS11b/TIS11d phosphospecific antibodies

Polyclonal phosphospecific antibodies against TIS11b-phospho-S54 and TIS11b-phospho-S334 were generated by injection of the synthetic keyhole limpet hemocyanin–conjugated peptides CAGGGFPRRH(Sp)VTL or RRLPIFSRL(Sp)ISD, respectively, into rabbits (CovalAb, Lyon, France). Sera were affinity purified using the same peptide, and nonphosphospecific antibodies were depleted by affinity purification using peptides containing unmodified serines. Due to the conservation of these sequences between TIS11b and TIS11d, the anti-phosphoserine antibodies recognized both phosphoproteins.

SDS–PAGE analysis and Western blot

SDS–PAGE analysis and Western blotting were performed as described previously (Planel *et al.*, 2010) using 4–20% gradient Mini-Protean TGX precast gels (Bio-Rad, Marnes-La-Coquette, France). The N- and C-terminal peptides from TIS11b were resolved on 16.5% Mini-Protean Tris-Tricine precast gels (Bio-Rad) and transferred on 0.2-μm-pore-size nitrocellulose sheets (Bio-Rad). In addition to the anti–phospho-TIS11b antibodies, the following antibodies were used: rabbit anti-TIS11b/TIS11d (BRF1/BRF2) (C. Moroni, University of Basel, Switzerland), mouse monoclonal anti-actin (Sigma-Aldrich), rabbit polyclonal anti-human Cnot1 (Proteintech, Manchester, UK), rabbit polyclonal anti-human Xrn1 (Abcam, Paris, France), rabbit polyclonal anti-human Dcp1a (Abcam), and rabbit polyclonal anti-human Dcp2 (Abcam). Blots were visualized and quantified using the ChemiDoc MP imaging system with Image Lab software (Bio-Rad).

Measurement of TIS11b protein and VEGF mRNA half-lives

COS7 cells (1.5×10^5) were seeded into 12-well plates and transfected 1 d later with 5–10 ng of pTarget-TIS11b plasmids (pTarget-WT, pTarget-TIS11b-S54A, pTarget-TIS11b-S54D, pTarget-TIS11b-S334A, or pTarget-TIS11b-S334D) using Lipofectamine (Invitrogen) according to the manufacturer's recommendations. At 48 h post-transfection, cycloheximide (10 μg/ml) or DRB (50 μg/ml) were added to each well for various periods of time. Cells were washed with cold PBS and lysed in RIPA buffer for protein extraction. Lysates were centrifuged at $10{,}000 \times g$ for 15 min at 4°C, and then protein concentration was determined using the Micro BCA Protein Assay Kit (Thermo Fisher, Illkirch, France). Total RNA isolation was carried out using the Nucleospin RNA extraction kit (Macherey Nagel, Düren, Germany) according to the manufacturer's instructions. Protein or RNA samples were subsequently analyzed by Western or Northern blotting, respectively (Planel *et al.*, 2010). The half-lives for TIS11b protein or VEGF mRNA were calculated using nonlinear regression to a first-order exponential decay model (GraphPad Prism, San Diego, CA). Half-lives were derived from the decay constant k ($t_{1/2} = \ln 2/k$).

Immunoprecipitation assays

HEK 293T cells cultured in 10 cm Petri dishes (4.5×10^6 cells/dish) were transfected with 250 ng of pTarget-TIS11b or pTarget-TIS11b mutant constructs. Total-cell lysates were cleared by centrifugation for 15 min at $12{,}000 \times g$ at 4°C. A mixture of rabbit antibodies targeting N-terminal and C-terminal peptide fragments of TIS11b (1 μg/ml) (Planel *et al.*, 2010) and anti-TIS11b/BRF1 polyclonal antibody (1/200 dilution; M. Schmidlin, University of Basel, Switzerland) was added to whole supernatants, which were then gently rocked overnight at 4°C before being incubated for 2 h with rabbit immunoglobulin G (IgG) TrueBlot beads (Tebu-Bio, Le Perray en Yvelines, France). Immunoprecipitates were pelleted, washed four times with RIPA buffer, analyzed by SDS–PAGE, and transferred to polyvinylidene fluoride membranes. Blots were probed with anti-TIS11b, anti-Cnot1, anti-Dcp1a, anti-Dcp2, or anti-Xrn1 antibodies. The membranes were thoroughly washed with Tris-buffered saline containing 0.1% Tween20, then incubated for 1 h with horseradish peroxidase–conjugated IgG fraction monoclonal mouse anti-rabbit IgG light chain-specific antibodies (Jackson ImmunoResearch, West Grove, PA). Blots were visualized and quantified using the ChemiDoc MP imaging system and the Image Lab software (Bio-Rad).

Statistical analysis

Statistical analysis was carried out using GraphPad Prism software. Data were analyzed using one-way analysis of variance (ANOVA). Results are expressed as means ± SEM. A value of $p < 0.05$ was considered statistically significant.

ACKNOWLEDGMENTS

This work was supported by the Institut National de la Santé et de la Recherche Médicale, the Commissariat à l'Energie Atomique et aux Energies Alternatives (International PhD Program IRTELIS to F.R.), and the Fondation pour la Recherche Médicale (to F.R. and S.P.). We thank C. Moroni and M. Schmidlin (University of Basel, Switzerland) for their generous gift of anti-TIS11b/TIS11d and anti-TIS11b antibodies.

REFERENCES

Baou M, Jewell A, Murphy JJ (2009). TIS11 family proteins and their roles in posttranscriptional gene regulation. J Biomed Biotechnol 2009, 634520.

Bell SE, Sanchez MJ, Spasic-Boskovic O, Santalucia T, Gambardella L, Burton GJ, Murphy JJ, Norton JD, Clark AR, Turner M (2006). The RNA binding protein Zfp36l1 is required for normal vascularisation and post-transcriptionally regulates VEGF expression. Dev Dyn 235, 3144–3155.

Benjamin D, Schmidlin M, Min L, Gross B, Moroni C (2006). BRF1 protein turnover and mRNA decay activity are regulated by protein kinase B at the same phosphorylation sites. Mol Cell Biol 26, 9497–9507.

Blackshear PJ, Phillips RS, Ghosh S, Ramos SB, Richfield EK, Lai WS (2005). Zfp36l3, a rodent X chromosome gene encoding a placenta-specific member of the Tristetraprolin family of CCCH tandem zinc finger proteins. Biol Reprod 73, 297–307.

Briata P, Chen CY, Ramos A, Gherzi R (2013). Functional and molecular insights into KSRP function in mRNA decay. Biochim Biophys Acta 1829, 689–694.

Brook M, Tchen CR, Santalucia T, McIlrath J, Arthur JS, Saklatvala J, Clark AR (2006). Posttranslational regulation of tristetraprolin subcellular localization and protein stability by p38 mitogen-activated protein kinase and extracellular signal-regulated kinase pathways. Mol Cell Biol 26, 2408–2418.

Brooks SA, Blackshear PJ (2013). Tristetraprolin (TTP): interactions with mRNA and proteins, and current thoughts on mechanisms of action. Biochim Biophys Acta 1829, 666–679.

Cao H, Deterding LJ, Blackshear PJ (2014). Identification of a major phosphopeptide in human tristetraprolin by phosphopeptide mapping and mass spectrometry. PLoS One 9, e100977.

Carballo E, Lai WS, Blackshear PJ (1998). Feedback inhibition of macrophage tumor necrosis factor-alpha production by tristetraprolin. Science 281, 1001–1005.

Carballo E, Lai WS, Blackshear PJ (2000). Evidence that tristetraprolin is a physiological regulator of granulocyte-macrophage colony-stimulating factor messenger RNA deadenylation and stability. Blood 95, 1891–1899.

Chamboredon S, Ciais D, Desroches-Castan A, Savi P, Bono F, Feige JJ, Cherradi N (2011). Hypoxia-inducible factor-1alpha mRNA: a new target for destabilization by tristetraprolin in endothelial cells. Mol Biol Cell 22, 3366–3378.

Cherradi N, Lejczak C, Desroches-Castan A, Feige JJ (2006). Antagonistic functions of tetradecanoyl phorbol acetate-inducible-sequence 11b and HuR in the hormonal regulation of vascular endothelial growth factor messenger ribonucleic acid stability by adrenocorticotropin. Mol Endocrinol 20, 916–930.

Chinn AM, Ciais D, Bailly S, Chambaz E, LaMarre J, Feige JJ (2002). Identification of two novel ACTH-responsive genes encoding manganese-dependent superoxide dismutase (SOD2) and the zinc finger protein TIS11b [tetradecanoyl phorbol acetate (TPA)-inducible sequence 11b]. Mol Endocrinol 16, 1417–1427.

Chrestensen CA, Schroeder MJ, Shabanowitz J, Hunt DF, Pelo JW, Worthington MT, Sturgill TW (2004). MAPKAP kinase 2 phosphorylates tristetraprolin on in vivo sites including Ser178, a site required for 14-3-3 binding. J Biol Chem 279, 10176–10184.

Ciais D, Cherradi N, Bailly S, Grenier E, Berra E, Pouyssegur J, Lamarre J, Feige JJ (2004). Destabilization of vascular endothelial growth factor mRNA by the zinc-finger protein TIS11b. Oncogene 23, 8673–8680.

Clement SL, Scheckel C, Stoecklin G, Lykke-Andersen J (2011). Phosphorylation of tristetraprolin by MK2 impairs AU-rich element mRNA decay by preventing deadenylase recruitment. Mol Cell Biol 31, 256–266.

Corps AN, Pascall JC, Hadfield KM, Brown KD (1995). Identification of a functional promoter element in the 5′-flanking region of the rat cMG1/TIS11b gene. Biochem J 311, 251–258.

Duan H, Cherradi N, Feige JJ, Jefcoate C (2009). cAMP-dependent post-transcriptional regulation of steroidogenic acute regulatory (STAR) protein by the zinc finger protein ZFP36L1/TIS11b. Mol Endocrinol 23, 497–509.

Duperray A, Chambaz EM (1980). Effect of prostaglandin E1 and ACTH on proliferation and steroidogenic activity of bovine adreno-cortical cells in primary culture. J Steroid Biochem 13, 1359–1364.

Fabian MR, Frank F, Rouya C, Siddiqui N, Lai WS, Karetnikov A, Blackshear PJ, Nagar B, Sonenberg N (2013). Structural basis for the recruitment of the human CCR4-NOT deadenylase complex by tristetraprolin. Nat Struct Mol Biol 20, 735–739.

Fan XC, Steitz JA (1998). Overexpression of HuR, a nuclear-cytoplasmic shuttling protein, increases the in vivo stability of ARE-containing mRNAs. EMBO J 17, 3448–3460.

Fenger-Gron M, Fillman C, Norrild B, Lykke-Andersen J (2005). Multiple processing body factors and the ARE binding protein TTP activate mRNA decapping. Mol Cell 20, 905–915.

Garneau NL, Wilusz J, Wilusz CJ (2007). The highways and byways of mRNA decay. Nat Rev Mol Cell Biol 8, 113–126.

Goldstrohm AC, Wickens M (2008). Multifunctional deadenylase complexes diversify mRNA control. Nat Rev Mol Cell Biol 9, 337–344.

Hsu PP, Kang SA, Rameseder J, Zhang Y, Ottina KA, Lim D, Peterson TR, Choi Y, Gray NS, Yaffe MB, *et al.* (2011). The mTOR-regulated phosphoproteome reveals a mechanism of mTORC1-mediated inhibition of growth factor signaling. Science 332, 1317–1322.

Kim TW, Yim S, Choi BJ, Jang Y, Lee JJ, Sohn BH, Yoo HS, Yeom YI, Park KC (2010). Tristetraprolin regulates the stability of HIF-1alpha mRNA during prolonged hypoxia. Biochem Biophys Res Commun 391, 963–968.

Kotlyarov A, Neininger A, Schubert C, Eckert R, Birchmeier C, Volk HD, Gaestel M (1999). MAPKAP kinase 2 is essential for LPS-induced TNF-alpha biosynthesis. Nat Cell Biol 1, 94–97.

Lykke-Andersen J, Wagner E (2005). Recruitment and activation of mRNA decay enzymes by two ARE-mediated decay activation domains in the proteins TTP and BRF-1. Genes Dev 19, 351–361.

Maitra S, Chou CF, Luber CA, Lee KY, Mann M, Chen CY (2008). The AU-rich element mRNA decay-promoting activity of BRF1 is regulated by mitogen-activated protein kinase-activated protein kinase 2. RNA 14, 950–959.

Marchese FP, Aubareda A, Tudor C, Saklatvala J, Clark AR, Dean JL (2010). MAPKAP kinase 2 blocks tristetraprolin-directed mRNA decay by inhibiting CAF1 deadenylase recruitment. J Biol Chem 285, 27590–27600.

Meisner NC, Filipowicz W (2010). Properties of the regulatory RNA-binding protein HuR and its role in controlling miRNA repression. Adv Exp Med Biol 700, 106–123.

Neininger A, Kontoyiannis D, Kotlyarov A, Winzen R, Eckert R, Volk HD, Holtmann H, Kollias G, Gaestel M (2002). MK2 targets AU-rich elements and regulates biosynthesis of tumor necrosis factor and interleukin-6 independently at different post-transcriptional levels. J Biol Chem 277, 3065–3068.

Ogilvie RL, Abelson M, Hau HH, Vlasova I, Blackshear PJ, Bohjanen PR (2005). Tristetraprolin down-regulates IL-2 gene expression through AU-rich element-mediated mRNA decay. J Immunol 174, 953–961.

Planel S, Salomon A, Jalinot P, Feige JJ, Cherradi N (2010). A novel concept in antiangiogenic and antitumoral therapy: multitarget destabilization of short-lived mRNAs by the zinc finger protein ZFP36L1. Oncogene 29, 5989–6003.

Sandler H, Kreth J, Timmers HT, Stoecklin G (2011). Not1 mediates recruitment of the deadenylase Caf1 to mRNAs targeted for degradation by tristetraprolin. Nucleic Acids Res 39, 4373–4386.

Schmidlin M, Lu M, Leuenberger SA, Stoecklin G, Mallaun M, Gross B, Gherzi R, Hess D, Hemmings BA, Moroni C (2004). The ARE-dependent mRNA-destabilizing activity of BRF1 is regulated by protein kinase B. EMBO J 23, 4760–4769.

She M, Decker CJ, Svergun DI, Round A, Chen N, Muhlrad D, Parker R, Song H (2008). Structural basis of dcp2 recognition and activation by dcp1. Mol Cell 29, 337–349.

Sinha S, Dutta S, Datta K, Ghosh AK, Mukhopadhyay D (2009). Von Hippel-Lindau gene product modulates TIS11B expression in renal cell carcinoma: impact on vascular endothelial growth factor expression in hypoxia. J Biol Chem 284, 32610–32618.

Stoecklin G, Stubbs T, Kedersha N, Wax S, Rigby WF, Blackwell TK, Anderson P (2004). MK2-induced tristetraprolin:14-3-3 complexes prevent stress granule association and ARE-mRNA decay. EMBO J 23, 1313–1324.

Stoecklin G, Tenenbaum SA, Mayo T, Chittur SV, George AD, Baroni TE, Blackshear PJ, Anderson P (2008). Genome-wide analysis identifies

interleukin-10 mRNA as target of tristetraprolin. J Biol Chem 283, 11689–11699.
Stumpo DJ, Broxmeyer HE, Ward T, Cooper S, Hangoc G, Chung YJ, Shelley WC, Richfield EK, Ray MK, Yoder MC, *et al*. (2009). Targeted disruption of Zfp36l2, encoding a CCCH tandem zinc finger RNA-binding protein, results in defective hematopoiesis. Blood 114, 2401–2410.
Sun L, Stoecklin G, Van Way S, Hinkovska-Galcheva V, Guo RF, Anderson P, Shanley TP (2007). Tristetraprolin (TTP)-14-3-3 complex formation protects TTP from dephosphorylation by protein phosphatase 2a and stabilizes tumor necrosis factor-alpha mRNA. J Biol Chem 282, 3766–3777.
Taylor GA, Carballo E, Lee DM, Lai WS, Thompson MJ, Patel DD, Schenkman DI, Gilkeson GS, Broxmeyer HE, Haynes BF, Blackshear PJ (1996). A pathogenetic role for TNF alpha in the syndrome of cachexia, arthritis, autoimmunity resulting from tristetraprolin (TTP) deficiency. Immunity 4, 445–454.
van Dijk E, Cougot N, Meyer S, Babajko S, Wahle E, Seraphin B (2002). Human Dcp2: a catalytically active mRNA decapping enzyme located in specific cytoplasmic structures. EMBO J 21, 6915–6924.
Venigalla RK, Turner M (2012). RNA-binding proteins as a point of convergence of the PI3K and p38 MAPK pathways. Front Immunol 3, 398.
Viengchareun S, Lema I, Lamribet K, Keo V, Blanchard A, Cherradi N, Lombes M (2014). Hypertonicity compromises renal mineralocorticoid receptor signaling through Tis11b-mediated post-transcriptional control. J Am Soc Nephrol 25, 2213–2221.
White EJ, Brewer G, Wilson GM (2013). Post-transcriptional control of gene expression by AUF1: mechanisms, physiological targets, and regulation. Biochim Biophys Acta 1829, 680–688.